Journal of Statistical Physics, Vol. 84, Nos. 3/4, 1996

Collapse Transition of a Two-Dimensional Lattice Animal

Roberto N. Onody[1] and Ubiraci P. C. Neves[1]

Received February 28, 1995; final November 21, 1995

The phase diagram and the tricritical point of a collapsing lattice animal are studied through an extended series expansion of the isothermal compressibility K_T on a square lattice. As a function of the variables of fugacity and Boltzmann weight, K_T is investigated using partial differential approximant techniques. The characteristic flow pattern of partial differential approximant trajectories is determined for a stable fixed point. We obtain satisfactory estimates for the tricritical fugacity $x_t = 0.024 \pm 0.005$ and temperature $T_t = 0.54 \pm 0.04$. Taking into account only linear scaling fields, we are also able to get the scaling exponent $\gamma = 1.4 \pm 0.2$ and the crossover $\phi = 0.66 \pm 0.08$. Our results are in reasonable agreement with previous estimates in the literature.

KEY WORDS: Series expansion; tricritical point; collapse transition; partial differential approximants; lattice animal; branched polymer.

1. INTRODUCTION

Linear polymers have been studied for a long time both experimentally and theoretically (see ref. 1 and references therein). A linear polymer molecule in dilute solution in a good solvent can be modeled as a self-avoiding walk on a regular lattice. In this regime the interactions are mostly the excluded-volume ones. As the temperature or the quality of the solvent decreases, attractive forces become important and the polymer may collapse at the tricritical Flory θ point. The attractive forces are induced by interactions with the solvent.

Branched polymers are made of monomers with functionality greater than 2. Randomly branched polymers in dilute silution in a good solvent can be modeled as lattice animals. Lattice animals are connected clusters of

[1] Departamento de Física e Informática, Instituto de Física de São Carlos, Universidade de São Paulo, São Carlos, São Paulo, Brazil.

0022-4715/96/0800-0399$09.50/0

occupied lattice sites including branches or loops. The introduction of attractive monomer–monomer interaction between nearest neighbor sites may lead to a collapse of the lattice animal at low temperatures. Such a collapse can experimentally be found in gels, particularly in acrylamide gel in a water–acetone mixture, where the volume changes by a factor 10^3 and a combined collapse and reswelling mechanism was found recently.[2] Theoretical evidence for this transition has been provided by several techniques: transfer matrix in two-dimensional strips,[1] Monte Carlo methods,[3,4] and series.[5–10] Dhar[11] proved the existence of the collapse transition in a related model—the two-dimensional directed lattice animal.

As the upper critical and tricritical dimensions are very high for the branched polymers ($d_c = 8$, $d_t = 6$), Flory arguments (mean field) are not expected to be as good as for the linear polymer case.

Besides being good models for branched polymers, lattice animals also appear in other physical situations, such as equilibrium DLA[12] and the study of vesicles.[13] The collapse of lattice animals may be driven by quite different agents: the number of interacting pairs of nearest neighbor sites in the animal, the number of cycles, or the number of nearest neighbor contacts (i.e., sites not directly connected by a bond belonging to the animal). The first two are equivalent[5] and there are recent claims of the exact determination of the critical exponents.[14] Contact models are believed to not belong to the same universality class as the pair or cycle models.[7]

In this paper our aim is to discuss the site lattice animal model defined on a square lattice and with attractive nearest neighbor pair interactions. In Section 2 we present the model and discuss some of its general features and behavior; in Section 3 we use a simple extrapolation algorithm to get the phase boundary. In Section 4 the partial differential approximant method is briefly introduced and applied to our model. The characteristic curves of a typical approximant are investigated in Section 5. The numerical estimates of the tricritical fugacity and temperature as well as the tricritical exponents are determined and they are then compared with the values obtained through other approaches. Finally, in Section 6 we summarize our results.

2. THE MODEL

Lattice animals can be classified into two different types: *site* and *bond* animals. A *site animal* is a connected section graph of the lattice so that if two vertices of the animal are on adjacent lattice sites they *must* be connected by an edge in the animal. A *bond animal* is a connected subgraph of the lattice so that two adjacent vertices of the animal *may* or *may not* be connected by an edge in the animal. A pair of two nearest neighbor sites

not directly connected by a bond belonging to the animal forms a *contact*. For site animals the number of contacts is zero, since contact models can only be constructed for bond animals.[6]

Recently an exhaustive exact enumeration of lattice animals was carried out in both square and cubic lattices.[6] The animals were classified by their numbers of vertices (up to size 19 for the square lattice), edges, and contacts. In our study, we consider one single cluster of N connected sites, i.e., one site animal, defined on a square lattice. Each pair of nearest neighbor sites has an additional attractive energy and the energy of the whole lattice animal is just the number of all pairs of nearest neighbors.[1] From Appendix A of ref. 6 we can extract the number $a_{N,m}$ corresponding to *site* animals (on the square lattice) with N vertices, m edges, and, of course, no contacts. For site animals, m coincides with the number of pairs of nearest neighbor sites. In this way, we can construct the grand partition function

$$G(x, y) = 1 + \sum_{N=1}^{19} \sum_{m=0}^{18} a_{N,m} x^N y^m$$
$$= 1 + x + 2x^2y + 6x^3y + x^4y^3(y + 18) + \cdots \tag{1}$$

where $x = \exp(\beta\mu)$ is the fugacity ($x < 1$; we use the same notation as in ref. 1), $y = \exp(1/T)$ is the Boltzmann weight ($y > 1$, so as to ensure an *attractive* pair interaction), and T is the reduced temperature.

We have truncated the power series up to order 18 in the variable y for a simple reason: animals with size $N \geqslant 20$ do *not* contribute to order $m \leqslant 18$ in the variable y.

From the generating function $G(x, y)$ we can derive the density

$$\rho \sim \langle N \rangle = \frac{x}{G} \frac{\partial G}{\partial x} \tag{2}$$

and the fluctuation or isothermal compressibility

$$K_T \sim \langle N^2 \rangle - \langle N \rangle^2 = x \frac{\partial \rho}{\partial x} \tag{3}$$

Formulas (2) and (3) can be implemented using symbolic computation software (e.g., MAPLE[2]). In Fig. 1 we plot ρ and K_T versus T for some fixed values of x. For small x the order parameter ρ evolves from a discontinuous jump (typical of a first-order phase transition) to a continuous

[2] MAPLE, copyright by the University of Waterloo, is a registered trademark of Waterloo Maple Software.

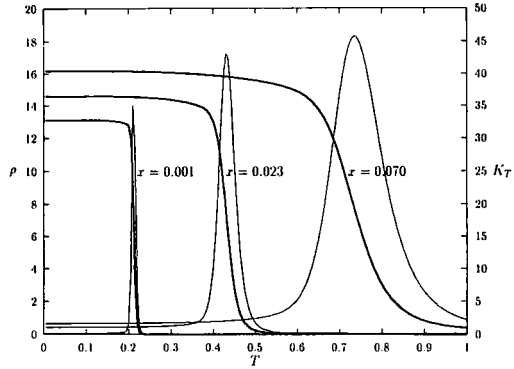

Fig. 1. Density ρ (thick lines) and isothermal compressibility K_T (thin lines) versus temperature T for some chosen fugacities x. The graph was obtained using a site lattice animal with size $N = 19$.

behavior for higher x values. This is a clue to the presence of a tricritical temperature. Also, the isothermal compressibility seems to exhibit, in the thermodynamic limit, a change from a delta-function to a power-law singularity.

3. FINITE-SIZE EXTRAPOLATION

Finite-size scaling theory attempts to describe how large-scale collective phenomena, associated with the onset of divergent fluctuations near critical points, manifest themselves in small samples.[15] For different lattice sizes physical quantities may be obtained and their values conveniently extended using some reliable extrapolation algorithm.

In our case, the size of the animal N (i.e., the number of sites belonging to the animal) can be fixed and the corresponding (truncated) formulas (1) and (3) can be calculated.

For *any* value of the fugacity x, we can determine the temperature T which maximizes the isothermal compressibility K_T. The plot of x versus T yields the "phase boundary" for that finite value N (see Fig. 2). Thus, for fixed x and different values of N, we can obtain a sequence $T^{(N)}$ of "critical temperatures." The extrapolated temperature of this sequence will determine the phase boundary of a system of infinite size.

We will assume that the sequence $T^{(N)}$ has the following asymptotic form ($N \to \infty$):

$$T^{(N)} = T_c + a_1 N^{-\omega} + a_2 N^{-2\omega} + \cdots \tag{4}$$

with a power-law dependence expected at the critical temperature.

Of the algorithms at our disposal[16] we have concentrated on two: the van den Broeck and Schwartz[17] (hereafter referred to as VBS) and the Bulirsch and Stoer[18] (hereafter referred to as BST) algorithms. To extrapolate our sequence we have chosen the BST algorithm for the following reasons: it does not require a consecutive sequence of finite data, i.e., it is more flexible than the VBS algorithm, and its convergence is also faster and is less sensitive to rounding errors.

We have considered (for each fixed fugacity x) a sequence of "critical temperatures" $T^{(N)}$ corresponding to values $N=7$, 10, 13, 16, and 19. The desired limit T_c of Eq. (4) was obtained from a table of extrapolants constructed according to the BST algorithm. The error in the determination of T_c is defined as the modulus of the difference between the two extrapolated temperatures at the penultimate stage of the algorithm.[16] The exponent ω is a free parameter which we allowed to assume different values for a determined sequence to be extrapolated. Minimizing the error yields an intrinsic criterion for choosing ω. Indeed, for each fugacity x, we selected the exponent ω which minimized this error.

In Fig. 2 we show the phase diagrams corresponding to the finite values $N=7$, 10, 13, 16, and 19 (thin lines). Using the least square method, we fitted the best curve to the extrapolated temperatures obtained through the BST algorithm. This curve corresponds to the phase boundary of a system of infinite size and is also shown in Fig. 2 (thick line). It separates the swollen phase from the collapsed one and is in good agreement with the phase diagram obtained through the transfer matrix technique.[1]

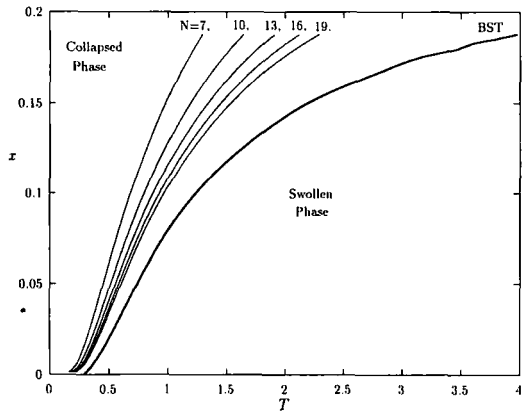

Fig. 2. Phase diagram computed via the BST extrapolation algorithm (thick line). The phase diagrams corresponding to the finite values $N=7$, 10, 13, 16, and 19 are also shown (thin lines).

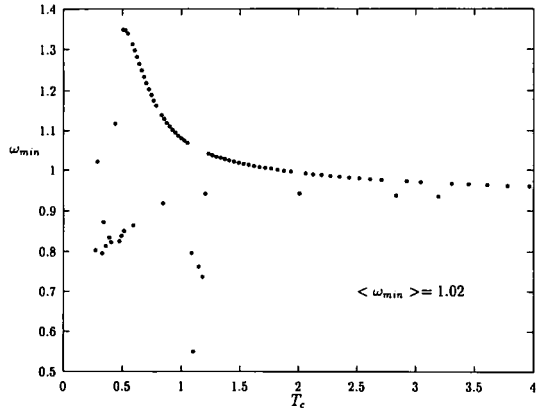

Fig. 3. Exponent $\omega_{\min}$, which minimizes the error in the BST extrapolation, as a function of the extrapolated temperature T_c.

However, the exact position of the tricritical point on the phase boundary is very difficult to obtain, so, for this purpose, we will apply the partial differential approximant technique in the next section.

In Fig. 3 we plot the exponent $\omega_{\min}$ corresponding to the minimum error against the extrapolated temperature T_c. We remark that ω is only an *effective* exponent, since Eq. (4) is valid only in the asymptotic limit. Large fluctuations appear near the tricritical temperature $T_t \sim 0.5$ and the values seem to go asymptotically to $\omega_{\min} \sim 0.95$ for the high-temperature region where a second-order phase transition takes place. We found the mean value $\langle \omega_{\min} \rangle = 1.02$ in the temperature interval $[0, 4]$. The increase of $\omega_{\min}$ close to $T_t \sim 0.5$ is certainly a clue to the presence of the tricritical point.

4. PARTIAL DIFFERENTIAL APPROXIMANTS

The concept of partial differential approximants was introduced by Fisher some time ago.[19] A partial differential approximant (PDA) provides a means of extrapolating the information embodied in the coefficients of a given double power series expansion. It is an appropriate tool in the study of functions which display intrinsically many-variable singularities. In particular, one may hope to extract reliable estimates for the location and the scaling exponents of the multisingular points.[20–25]

A partial differential approximant to a function $f(x, y)$ is the solution $F(x, y) \equiv F_{K:MNLJ}(x, y)$, satisfying appropriate boundary conditions, of the defining equation

$$Q_M(x, y)\frac{\partial F(x, y)}{\partial x} + R_N(x, y)\frac{\partial F(x, y)}{\partial y} = P_L(x, y)\,F(x, y) + U_J(x, y) \quad (5)$$

Here the polynomials Q_M, R_N, P_L, and U_J ($Q_M = \sum_{(m, m') \in M} q_{m, m'} x^m y^{m'}$, etc.) contain only powers defined by the *label sets* $M \supset (m, m')$, $N \supset (n, n')$, $L \supset (l, l')$, and $J \supset (j, j')$. Their coefficients $q_{m, m'}$, $r_{n, n'}$, $p_{l, l'}$, and $u_{j, j'}$ are obtained by solving linear algebraic equations chosen so that the power series expansion of $F(x, y)$ reproduces the known series $f(x, y) = \sum_{(i, i') \in I} f_{i, i'} x^i y^{i'}$ to an acceptable degree. The coefficients $f_{i, i'}$ are known only for (i, i') belonging to some finite label set I (*index set*); the generating equations for the polynomial coefficients follow from demanding that when $F(x, y)$ is replaced by $f(x, y)$ in (5), the power series expansion of both sides agree in all orders $x^k y^{k'}$ for which (k, k') lies in a prescribed *matching label set* K (see ref. 21 for further details).

The multisingular point (x_c, y_c) is determined by the fixed-point equations

$$Q_M(x_c, y_c) = R_N(x_c, y_c) = 0 \quad (6)$$

In general $F(x, y)$ obeys an asymptotic scaling law which may be written in the canonical form

$$F(x, y) \sim |\tilde{x}|^{-\gamma} Z(\tilde{y}/|\tilde{x}|^{\phi}) + B \quad (7)$$

where γ is the *scaling* exponent, ϕ is the *crossover* exponent, B represents the so-called background amplitude, and $\tilde{x}$ and $\tilde{y}$ are termed linear scaling fields given by the linear combinations

$$\tilde{x} = \Delta x - \Delta y/e_2 \qquad \text{and} \qquad \tilde{y} = \Delta y - e_1\,\Delta x \quad (8)$$

with $\Delta x = x - x_c$ and $\Delta y = y - y_c$. The slopes e_1 and e_2 of the scaling axes must be the roots of

$$Q_y e^2 + (Q_x - R_y)\,e - R_x = 0 \quad (9)$$

where Q_x, Q_y, R_x, R_y are partial derivatives with respect to x and y evaluated at the multicritical point (x_c, y_c).

The most appropriate method of solving the defining partial differential equation (5) is through an integration along the characteristics. These

may be constructed by defining a timelike variable τ and solving the ordinary differential equations

$$\frac{dx}{d\tau} = Q_M(x, y) \qquad \text{and} \qquad \frac{dy}{d\tau} = R_N(x, y) \tag{10}$$

If we linearize around the multicritical point (x_c, y_c) the equations above can be written as

$$\frac{d\tilde{x}}{d\tau} = \lambda_1 \tilde{x} \qquad \text{and} \qquad \frac{d\tilde{y}}{d\tau} = \lambda_2 \tilde{y} \tag{11}$$

where

$$\lambda_1 = Q_x - R_x/e_2 \qquad \text{and} \qquad \lambda_2 = R_y - e_1 Q_y \tag{12}$$

When *both* λ_1 and λ_2 are positive (negative) we call (x_c, y_c) an unstable (stable) point; when they have opposite signs we denote it a saddle point, whereas in situations where the solutions of Eq. (9) become complex we call it a spiral point.

We can get the exponents from the expressions

$$\phi = \lambda_2/\lambda_1 \qquad \text{and} \qquad \gamma = P_0/\lambda_1 \tag{13}$$

We have applied the PDA technique to study the multisingular properties of the isothermal compressibility K_T as a function of the fugacity x and the Boltzmann weight y. Our results are presented in the next section.

5. NUMERICAL RESULTS

In the application of the PDA technique, it is necessary to choose the nonzero powers of the polynomial label sets M, N, L, J and of the matching label set K. Important guidance for the choice of these label sets is provided by theorems concerning faithfulness and invariance properties of PDAs.[21] An approximant $F(x, y)$ is *faithful* if each coefficient $F_{i,i'}$ of its series expansion is equal to $f_{i,i'}$ for all the $f_{i,i'}$ that were needed to compute $F(x, y)$. Faithfulness is clearly a desirable property for an approximant. It can be ensured by imposing the proper boundary conditions and by picking a matching label set K of an appropriate shape. Another important property is the invariance of approximants under Euler transformations $[x \to \bar{x} = Ax/(1 + Bx)]$. Approximants conforming or nearly conforming to the requirements for Eulerian invariance provide more reliable and stable

estimates for the properties of the function in question. In fact this seems to be confirmed in the present work as well as in the practical calculations of refs. 19 and 22. Invariance hinges on appropriate choice of the label sets M, N, L, J, and K.

In many series that arise in practical applications a large fraction of the coefficients $f_{i,i'}$ are known to vanish identically. For example, the upper triangular series analyzed by Chen *et al.*[22] have $f_{i,i'} \equiv 0$ for $i < i'$. In other cases, $x^{\bar{i}} f(x, y)$ may be upper triangular for some positive or negative integer $\bar{i}$, and so on. In ref. 21, well-developed theorems are given that can be applied to upper triangular functions: Theorem 3.7 establishes the appropriate shapes for the label sets so as to ensure that the approximant is faithful provided $p_{0,0} - hq_{1,0} - h'r_{0,1} \neq 0$ (where h and h' are nonnegative integers). Theorem 6.3 presents quite compatible criteria for Euler invariance.

We have studied the critical behavior of the isothermal compressibility K_T through the PDA technique. Due to the upper triangular character of $f = x^5 K_T(x, y)$, the shapes of the polynomial label sets M, N, L, J and of the matching label set K were chosen according to Theorems 3.7 and 6.3 of ref. 21 on faithfulness and on Euler invariance. However, for all allowed choices of K, this procedure led us to a set of equations which contained undesirable relations satisfying $p_{0,0} - hq_{1,0} - h'r_{0,1} = 0$ and thus violating one of the conditions for faithfulness. Nevertheless, the conditions for Eulerian invariance were still maintained, and this was certainly very important. As a matter of fact, in many works where the PDA method is applied, the selected approximants are exclusively Eulerian or near-Eulerian.[22, 23]

Specifically, Theorem 6.3 of ref. 21 on Euler invariance on x establishes that the label sets M, N, L, J must be contained in upper triangular arrays so that $m \geqslant m' + 1$, $n \geqslant n' - 1$, $l \geqslant l'$, and $j \geqslant j'$. An additional condition is $\hat{m} - 2 = \hat{n} = \hat{l} = \hat{j}$, where $\hat{m}$, $\hat{n}$, $\hat{l}$, and $\hat{j}$ are, respectively, the largest powers of x in the polynomials Q_M, R_N, P_L, and U_J. In addition, each row in the corresponding Cartesian arrays of these label sets must be *flush right*, i.e., a gapless sequence of elements running downward from the respective largest power of x to a lower limit. The matching set K should be upper triangular and *flush left*.

In this way, we then constructed the upper triangular arrays M_-, N_-, and L for the corresponding defining polynomials $Q_M = xQ_{M_-}^{-}(x, y)$, $R_N = yR_{N_-}^{-}(x, y)$, and P_L, with $\hat{m} - 2 = \hat{n} = \hat{l} = 9$. This is compatible with the requirements on Euler invariance. Since for strongly divergent functions like K_T the background term U_J would not normally be so important, we have made $U_J = 0$. This spoils *precise* Eulerian invariance (although a homogeneous PDA with $U_J = 0$ *can* be Euler invariant); however, it seems

to be better to allow larger arrays M and N, in particular, since these determine the *flow patterns* of the characteristic trajectories and thence the critical locus (as will be exposed later).

The standard normalization $p_{0,0}=1$ was used in order to obtain a set of nonhomogeneous linear equations. To avoid an over- or underdetermined set of algebraic equations, the number of linearly independent equations must clearly equal the number of unknown polynomial coefficients. The generating equations for the polynomial coefficients were solved with help of MAPLE for different choices of matching label sets compatible with the theorem on Euler invariance.

We computed a total of 210 near-Eulerian approximants,[3] 109 of them exhibing the multicritical point (the crossing of zero loci $Q_M=R_N=0$) in the intervals $0.015<x<0.035$ and $y>1$. One should observe that a singularity in the region $y<1$ would correspond to the sector of repulsive monomer–monomer interactions. From these multicritical points, 90 are stable points (82.6%), 13 are saddle points (11.9%), and 6 are spiral points (5.5%).

One observes that defining a multisingular point as being stable or unstable is only a matter of the sign of τ in Eq. (11).[24] On the other hand, saddle points correspond to a negative crossover exponent ϕ. They are associated with corrections to scaling[23] where irrelevant operators give rise to contributions (with nonintegral powers) to the expansion of some thermodynamic quantity near a critical point. The spiral points correspond to nonphysical singularities and should be rejected.

The solution of the ordinary differential equations (10) with given initial conditions specifies a definite *trajectory* in the (x, y) plane. The set of all trajectories defines a flow pattern which is characteristic of the approximant in question. We have found some characteristic curves for a typical stable point approximant by solving numerically the corresponding equations (10) through a Fehlberg fourth-fifth-order Runge-Kutta method. The characteistic flow pattern of this approximant in the (T, x) plane is shown in Fig. 4. The loci of $Q=0$ and $R=0$ are represented by dotted curves. Their intersection determines the multicritical point C. The straight lines describe the tangents of the scaling axes $\tilde{x}$ and $\tilde{y}$ at point C in the (T, x) plane. The characteristic trajectories are shown by full lines labeled 1–7 in a clockwiselike manner. Curves 1–5 are tangent to the scaling axis $\tilde{y}$ at the multicritical point; they correspond to the critical trajectory. The arrows indicate the sense of the trajectories for increasing positive τ. Note

[3] In the literature, the use of near-invariant approximants is usually found to be entirely satisfactory. That is to say, those approximants that satisfy a variety of invariance requirements are not obviously better converged than their "near-invariant" neighbors.[25]

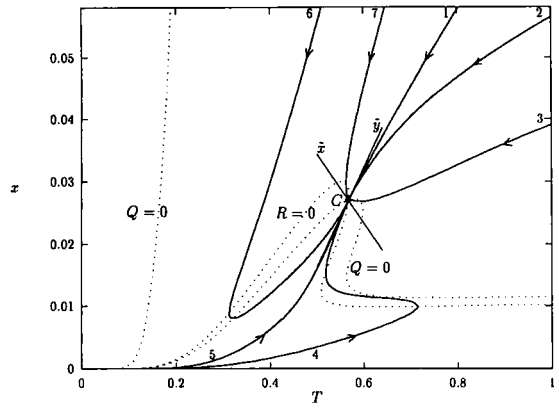

Fig. 4. Characteristic flow pattern of PDA trajectories for a typical stable-point ($\phi > 0$) approximant. Some characteristic curves (1–7) are shown by full lines. The loci of $Q=0$ and $R=0$ (dotted curves) intersect at the multicritical point C. The straight lines represent the tangents of the scaling axes $\tilde{x}$ and $\tilde{y}$ at point C in the (T, x) plane.

that the trajectories do not meet or cross except at the multisingular point(s) of the approximant. Since the slope dx/dT of each trajectory is proportional to Q_M/R_N, the arrangement of zero loci determines the overall topology of the flow pattern. In fact, one can observe in Fig. 4 that the slope of a trajectory passes through zero when it crosses a $Q=0$ locus, whereas the slope passes through infinity when a trajectory crosses an $R=0$ locus.

In Fig. 5, the critical trajectory corresponding to the same stable point is presented for larger intervals of temperature and fugacity. The loci of zeros and the tangents of the scaling axes at the multicritical point C are also plotted. Note that the critical line is in good accordance with that one extrapolated through the BST algorithm (Fig. 2).

We now average the relevant quantities in order to get an estimative of the tricritical fugacity x_t and temperature T_t. For this purpose, we discard the saddle points ($\phi < 0$) and the spiral points (nonphysical singularities). Fortunately, these represent only 17.4% of the total of multicritical points. The relevant multisingularities constitute the majority (82.6%) and correspond to stable points. Over this ensemble we obtain the averages and standard deviations of the tricritical fugacity and temperature

$$x_t = 0.024 \pm 0.005 \qquad \text{and} \qquad T_t = 0.54 \pm 0.04 \tag{14}$$

These results are in good agreement with (although with a larger standard deviation than) the values $x_t = 0.0230 \pm 0.0004$ and $T_t = 0.535 \pm 0.005$ obtained using transfer matrices for strips.[1]

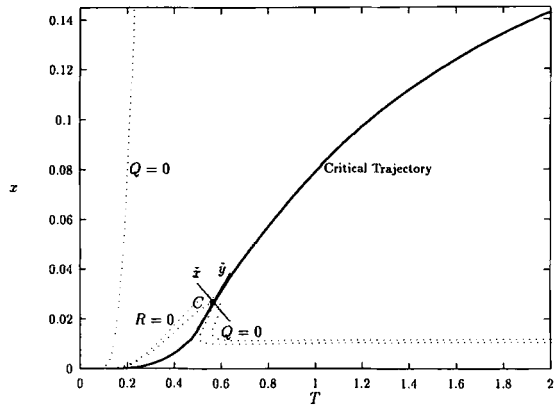

Fig. 5. Critical trajectory corresponding to the same stable-point approximant of Fig. 4, for larger intervals of temperature T and fugacity x. The loci of zeros (dotted curves) and the tangents of the scaling axes (straight lines) at C are also plotted.

With regard to the scaling exponents γ and ϕ, it is important to point out that the results of the linearized theory [formulas (11)–(13)] are fully valid only for values of the crossover ϕ lying in the interval $(1/2, 2)$; otherwise we must consider nonlinear scaling fields.[24]

In order to calculate the mean values of the exponents, we average them only over the approximants with ϕ in this restricted interval. The scaling and crossover exponents obtained are

$$\gamma = 1.4 \pm 0.2 \qquad \text{and} \qquad \phi = 0.66 \pm 0.08 \tag{15}$$

The crossover exponent is in good agreement with the value estimated by the transfer matrix method, namely, $\phi = 0.657 \pm 0.025$,[1] and with the proposed exact value $\phi = 2/3$.[14]

Additionally, we also explored the PDA technique by choosing other shapes for the label sets. Specifically, we selected square arrays. The criterion for this selection is *ad hoc*. However, it is worth comparing the results of both strategies. In this choice, the label sets M, N, and L are gapless square arrays with degrees $\hat{m} = \hat{n} = \hat{l} = 8$. The polynomial U_J is null and, as usual, $p_{0,0} = 1$. In the defining partial differential equation, $F(x, y)$ is then replaced by the series $K_T(x, y)$ known up to order $x^{19}y^{18}$. Due to the presence of derivatives in this equation, the elements (k, k') of the matching label set K are chosen in the ranges $0 \leqslant k \leqslant 18$ and $0 \leqslant k' \leqslant 17$. The equations originated from the smaller power coefficients are fixed and other equations coming from the larger set which includes higher power coefficients are added in a combined way. This procedure yielded 451

approximants exhibiting the expected tricritical points with the following profile: 15 stable points, 79 unstable points, and 357 saddle points (the nonphysical spiral points were rejected). Besides the expected tricritical point, most of the approximants present a plethora of other multicritical points in the (T, x) plane, some of them with a nonphysical nature. For example, a typical saddle-point approximant presents an extra fixed point D on the axis $x=0$, which can be regarded as a *defective* or *spurious* singularity since we know that the underlying function $K_T(x, y)$ is analytic in that region. Moreover, this point does not belong to the critical trajectory [which is tangent to the scaling axis $\tilde{y}$ at the *main* tricritical point $C \equiv (T_c, x_c)$]. There is another fixed point B on the critical trajectory, in the region $T < T_c$; it could, in principle, change the critical behavior along the locus CB. This kind of additional fixed point has already appeared in the literature.[23] It was called a *border* point and might be interpreted as a premature representation of an incipient tricritical point.

We have also studied the statistics of extra fixed points over the stable or unstable tricritical point approximants. Around 94% of these approximants contain defective points (distributed in all stable point approximants and in 73 of the unstable ones). The border points appear in 14.9% of these approximants (specifically, in 12 stable-point approximants and only in 2 unstable ones). Again, the averages of the relevant quantities were taken over this ensemble of approximants (saddle-point approximants were discarded). The estimatives of the tricritical fugacity and temperature are $x_t = 0.024 \pm 0.009$ and $T_t = 0.55 \pm 0.08$. The scaling and crossover exponents averaged over those approximants with ϕ in the interval $(1/2, 2)$ are $\gamma = 1.9 \pm 0.5$ and $\phi = 0.63 \pm 0.09$.

We can now compare these results with those obtained from the near-invariant approximants through Euler transformation [see Eqs. (14) and (15)]. The estimates resulting from the two strategies are in good agreement, but smaller standard deviations characterize the near-invariant approximants. Besides, as we have seen, the unreasonable cases (saddle multicritical points and defective points) are much more frequent in our "noninvariant" approximants. On the contrary, stable multicritical points constitute the majority in our near-Eulerian approximants. Once more, the importance of invariant approximants (which provide more reliable and stable estimates) has been noted. In this sense, the estimates in Eqs. (14) and (15) are the preferable results.

6. SUMMARY

We have presented a model with two parameters, temperature and fugacity, to describe the collapse transition of branched polymers. These

were treated as site lattice animals with attractive nearest neighbor pair interactions. Thanks to an exhaustive exact enumeration of these animals, we were able to write down the isothermal compressibility and to verify the existence of a tricritical point separating a region of a first-order phase transition from a second-order phase transition. A simple extrapolation algorithm gave us a sketch of the phase boundaries.

To study more deeply the tricritical point we have applied partial differential approximants to locate the singularity and to estimate the corresponding scaling exponents. The importance of the use of invariant approximants has been noted once more. The values we obtained are in good agreement with those derived from other techniques.

We hope our work will encourage more people to use the method, which is specially designed to treat multisingularities.

ACKNOWLEDGMENTS

We have benefitted from helpful discussions with Prof. S. R. Salinas and Dr. J. F. Stilck in many stages of the work reported here. We gratefully acknowledge financial support by CNPq (Conselho Nacional de Desenvolvimento Científico e Tecnológico).

REFERENCES

1. B. Derrida and H. J. Herrmann, *J. Phys.* (Paris) **44**:1365 (1983).
2. T. Ikehara and T. Nishi, *Phys. Rev. Lett.* **71**:2497 (1993).
3. R. Dickman and W. C. Shieve, *J. Phys.* (Paris) **45**:1727 (1984).
4. P. M. Lam, *Phys. Rev. B* **36**:6988 (1987); **38**:2813 (1988).
5. D. S. Gaunt and S. Flesia, *Physica A* **168**:602 (1990).
6. N. Madras, C. E. Soteros, S. G. Whittington, J. L. Martin, M. F. Sykes, S. Flesia, and D. S. Gaunt, *J. Phys. A* **23**:5327 (1990).
7. D. S. Gaunt, *Physica A* **177**:146 (1991).
8. S. Flesia and D. S. Gaunt, *J. Phys. A* **25**:2127 (1992).
9. S. Flesia, D. S. Gaunt, C. E. Soteros, and S. G. Whittington, *J. Phys. A* **25**:L1169 (1992).
10. S. Flesia, D. S. Gaunt, C. E. Soteros, and S. G. Whittington, *J. Phys. A* **26**:L993 (1993).
11. D. Dhar, *J. Phys. A* **20**:L847 (1987).
12. R. Wessel and R. C. Ball, *Phys. Rev. A* **45**:2177 (1992).
13. M. E. Fisher, A. J. Guttmann, and S. G. Whittington, *J. Phys. A* **24**:3095 (1991).
14. C. Vanderzande, *Phys. Rev. Lett.* **70**:3595 (1993).
15. V. Privman, ed., *Finite Size Scaling and Numerical Simulation on Statistical Systems* (World Scientific, Singapore, 1990).
16. M. Henkel and G. Schütz, *J. Phys. A* **21**:2617 (1988).
17. J. M. van den Broeck and L. W. Schwartz, *SIAM J. Math. Anal.* **10**:658 (1979).
18. R. Bulirsch and J. Stoer, *Numer. Math.* **6**:413 (1964).
19. M. E. Fisher, *Physica* **86–88**:590 (1977); M. E. Fisher and R. M. Kerr, *Phys. Rev. Lett.* **39**:667 (1977).

20. J. F. Stilck and S. R. Salinas, *J. Phys. A* **14**:2027 (1981).
21. M. E. Fisher and D. F. Styer, *Proc. R. Soc. Lond. A* **384**:259 (1982); D. F. Styer and M. E. Fisher, *Proc. R. Soc. Lond. A* **388**:75 (1983).
22. J.-H. Chen, M. E. Fisher, and B. G. Nickel, *Phys. Rev. Lett.* **48**:630 (1982).
23. M. Barma and M. E. Fisher, *Phys. Rev. B* **31**:5954 (1985).
24. M. Randeria and M. E. Fisher, *Proc. R. Soc. Lond. A* **419**:181 (1988).
25. A. J. Guttmann, In *Phase Transitions and Critical Phenomena*, Vol. 13, C. Domb and J. L. Lebowitz, eds. (Academic Press, New York, 1989).